Journal of
Materials Chemistry C

COMMUNICATION

View Article Online
View Journal

Cite this: DOI: 10.1039/c9tc00162j

Received 10th January 2019,
Accepted 28th February 2019

DOI: 10.1039/c9tc00162j

rsc.li/materials-c

A cyclopentadithiophene-bridged small molecule acceptor with near-infrared light absorption for efficient organic solar cells†

Yuan-Qiu-Qiang Yi, Huanran Feng, Xin Ke, Jing Yan, Meijia Chang, Xiangjian Wan, Chenxi Li and Yongsheng Chen *

A cyclopentadithiophene (DTC)-bridged acceptor–donor–acceptor (A–D–A) backboned small molecule acceptor (SMA), namely IDTC-4Cl, was designed and synthesized. In combination with strong electron-withdrawing (5,6-dichloro-3-oxo-2,3-dihydro-1*H*-indene-2,1-diylidene)dimalononitrile as a terminal group, IDTC-4Cl exhibits a near-infrared light absorption with an edge over 900 nm. Using PBDB-T as the polymer donor, the IDTC-4Cl based device gives a PCE of 9.51% with a V_{oc} of 0.822 V, FF of 60.2% and J_{sc} of 19.14 mA cm^{-2}. Upon introduction of PC$_{71}$BM as the third component, the ternary OSCs show an enhanced PCE of 10.41% with a much improved FF of 65.6%, which exemplifies the potential of utilizing a DTC unit to construct an SMA for high-performance organic photovoltaics.

Introductions

Organic solar cells (OSCs) have received tremendous attention in the last few decades for their great potential advantages of solution processibility, light weight, low cost and easy large area fabrication.[1–4] Recently, owing to the rapid development of non-fullerene small molecule acceptors (NF-SMAs) along with morphology control and device engineering, the power conversion efficiencies (PCEs) of single junction and double junctions OSCs have been boosted to over 14% and 17%, respectively.[5–10] Compared with the broad absorption spectrum within 1100 nm of single crystal silicon solar cells, the OSCs have a poor spectral response in this region.[11,12] Thus, organic semiconductors with a broad light absorption band in the vis-infrared (NIR) region are considered to harvest more solar photons to generate a high photocurrent, and, as a result, may contribute to an overall enhanced efficiency for OSCs.[4] Therefore, the design and synthesis of NIR materials with a narrow-bandgap (NBG) is expected to further enhance the performance of organic photovoltaics.

Among the most successful NF-SMAs, almost all contain a planar acceptor–donor–acceptor (A–D–A) backbone architecture, which is beneficial for fine-tuning energy levels, light absorption and enhanced intramolecular charge transfer (ICT) effect.[13–16] The most commonly reported highly efficient non-fullerene OSCs have limited photo-response coverage within 850 nm, using indacenodithiophene (IDT), indacenodithieno[3,2-*b*]-thiophene (IDTT) fluorenedicyclopentathiophene and heptacyclic benzodi-(cyclopentadithiophene) based NF-SMAs.[17–25] As such, further extending the spectral response in the NIR/IR region of OSCs is of great significance and interest for the design of NBG NF-SMAs for highly efficient OSCs. With these, there are some successful extreme-NBG SMA based OSCs with PCEs over 10%.[26–29]

Considering the requirements for NF-OSCs and pioneering works aforementioned, we envisioned that further extending an IDT core linked by more thiophene units together with using stronger electron-withdrawing end-groups may be a good choice for the design and synthesis of NBG NF-SMA materials. There are many successful NF-SMAs with good photovoltaic performance by utilization of IDT as the central donor core, such as IEIC, IEICO, IDTBR, IDT-2BR, ATT-1 and many analogues.[27,29–38] Furthermore, a cyclopentadithiophene (DTC) unit is of great interest for its suitable thiophene number and bulky substituents attached on the sp^3 carbon atoms. Recently, Chen *et al.* reported a DTC based unfused NF-SMA DF-PCIC for highly efficient OSCs, which proved that it is feasible to use DTC as a building block for constructing SMAs.[39,40] Side chains attached on the sp^3-carbon of IDT and DTC units together could guarantee avoiding strong intermolecular aggregation for achieving suitable phase separation domains and purity. Meanwhile, strong electron-withdrawing end-groups may contribute to favorable π–π stacking and enhanced intermolecular charge transfer.

In this work, we designed and synthesized a new NF-SMA, 2,2′-((2*Z*,2′*Z*)-(((4,4,9-tris(4-hexylphenyl)-9-(4-pentylphenyl)-4,9-dihydro-*s*-indaceno[1,2-*b*:5,6*b*]-dithiophene-2,7-diyl)bis(4,4-bis-(2-octyl)-4*H*-cyclopenta[2,1-*b*:3,4-*b*′]dithiophene-6,2-diyl))bis(meth-anylylidene))bis(5,6-dichloro-3-oxo-2,3-dihydro-1*H*-indene-2,1-diylidene))dimalononitrile (**IDTC-4Cl**), which possessed a narrow

Institute of Polymer Chemistry, Key Laboratory of Functional Polymer Chemistry, State Key Laboratory of Elemento-organic Chemistry, College of Chemistry, Nankai University, Tianjin, 300071, China. E-mail: yschen99@nankai.edu.cn

† Electronic supplementary information (ESI) available. See DOI: 10.1039/c9tc00162j

bandgap of 1.35 eV and effective light absorption from 700 to 900 nm in the near and far infrared regions. **IDTC-4Cl** employs IDT as the central core bridged by two cyclopentadithiophene (DTC) units and ends capped by two same strong electron-withdrawing terminal groups (5,6-dichloro-3-oxo-2,3-dihydro-1*H*-indene-2,1-diylidene)dimalononitrile (IC-2Cl), which could effectively decrease the lowest unoccupied molecular orbital (LUMO) level, increase the molecular crystallinity and enhance the charge transfer. From the perspectives of the energy levels and the light absorption of **IDTC-4Cl**, a medium bandgap polymer, poly[(2,6-(4,8-bis(5-(2-ethylhexyl)thiophen-2-yl)benzo[1,2-*b*:4,5-*b*′]-dithiophene)-*alt*-(1,3-di(5-thiophene-2-yl)-5,7-bis(2-ethylhexyl)benzo-[1,2-*c*:4,5-*c*′]dithiophene-4,8-dione))] (**PBDB-T**) was chosen as the electron donor to fabricate the OSC device with a complementary absorption in the visible and NIR regions. The **PBDB-T:IDTC-4Cl** based device delivered a PCE of 9.5%. In order to further elevate the photovoltaic performance, phenyl-C_{71}-butyric-acid-methyl ester ($PC_{71}BM$) was chosen as the third component to fabricate the OSC device. As expected, this ternary strategy gave an increased PCE of 10.41% and a low energy loss of 0.527 eV, together with a significant elevated FF from 60.2% to 65.2%, and an almost unchanged J_{sc} of 19.14 mA cm^{-2} and V_{oc} of 0.829 eV.

Synthesis and characterizations

The synthetic route of **IDTC-4Cl** is shown in Fig. 2, and the detailed synthesis procedures and characterization data are given in theESI.† The Stille cross-coupling reaction between commercially available (4,4,9,9-tetrakis(4-hexylphenyl)-4,9-dihydro-sindaceno[1,2-*b*:5,6-*b*′]dithiophene-2,7-diyl)bis(trimethylstannane) and 6-bromo-4,4-dioctyl-4*H*-cyclopenta[2,1-*b*:3,4-*b*′]dithiophene-2-carboxaldehyde, could generate an important intermediate dialdehyde IDTC-2CHO directly. The desired molecule **IDTC-4Cl** was then obtained by the Knoevenagel condensation reaction with IC-2Cl in a decent yield of 80%. **IDTC-4Cl** was fully characterized by ^{1}H, ^{13}C NMR, and high resolution mass spectrometry (HR-MS MALDI) as shown in the ESI.† Since **IDTC-4Cl** has eight side chains, it shows a very good solubility in common organic solvents (dichloromethane, chloroform and chlorobenzene). It should also be noticed that the eight bulky side chains can effectively avoid over strong aggregation in the solid state for an optimal morphology. **IDTC-4Cl** exhibited a decomposition temperature (T_d) of 370 °C with 5% weight loss determined from thermo-gravimetric analysis (TGA) curves (Fig. S1, ESI†), guaranteeing its good enough thermal stability for device fabrication.

Optical and electrochemical properties

As shown in Fig. 1d, the ultraviolet-visible (UV-Vis) absorption spectrum of **IDTC-4Cl** in a diluted $CHCl_3$ solution shows a major absorption peak at 780 nm, which shifts to 807 nm for the thin-film absorption of **IDTC-4Cl**, corresponding to a 27 nm bathochromic-shift compared with that of its chloroform solution, indicating a more-ordered structure and strong π–π intermolecular interaction in the thin film. Combining with the absorption of **PBDB-T** in the range of 450–700 nm, **IDTC-4Cl** exhibits a complementary absorption in the range of 700–910 nm which may favor complete harvesting of solar photons from the visible light to the NIR/IR region. The E_g^{opt} of **IDTC-4Cl**, calculated from its absorption onset of 914 nm, is as low as 1.35 eV. The UV-Vis absorption spectrum of blend films based on **IDTC-4Cl:PBDB-T** binary and **IDTC-4Cl:PBDB-T**:$PC_{71}BM$ ternary OSCs are shown in Fig. S4 (ESI†).

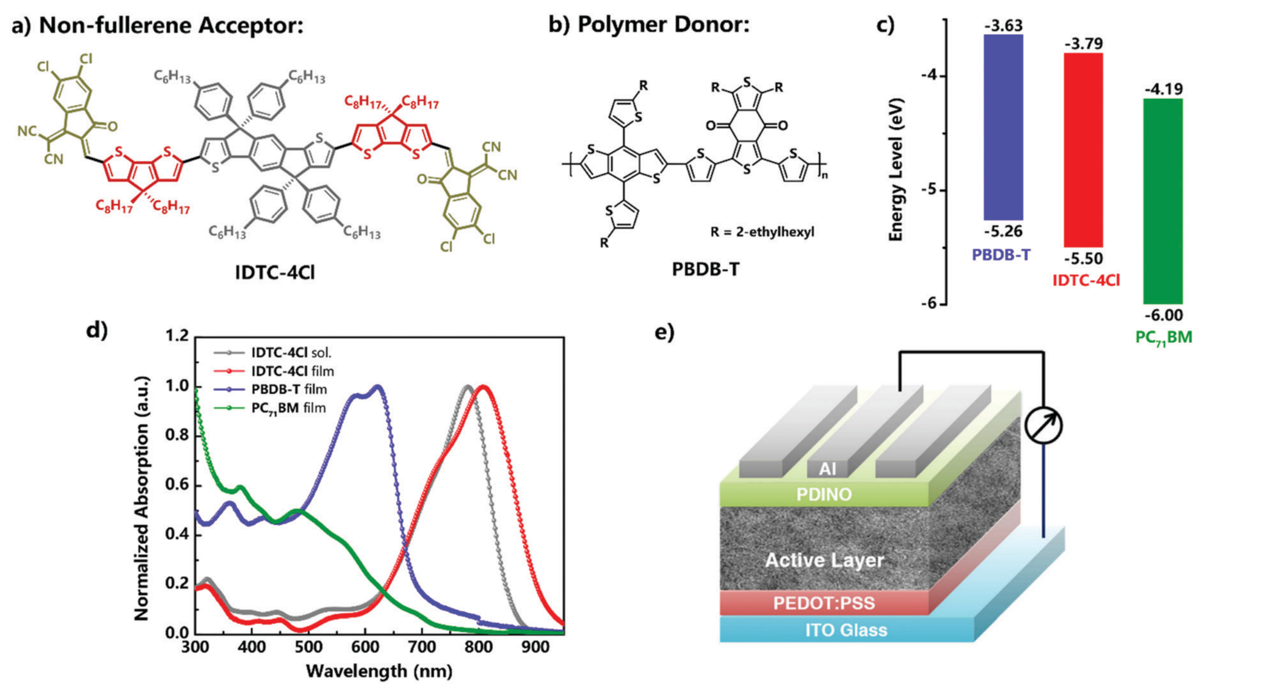

Fig. 1 Chemical structures of (a) **IDTC-4Cl** and (b) **PBDB-T**; (c) energy levels and (d) UV-Vis-NIR absorptions of **PBDB-T**, **IDTC-4Cl** and $PC_{71}BM$; (e) the device architecture.

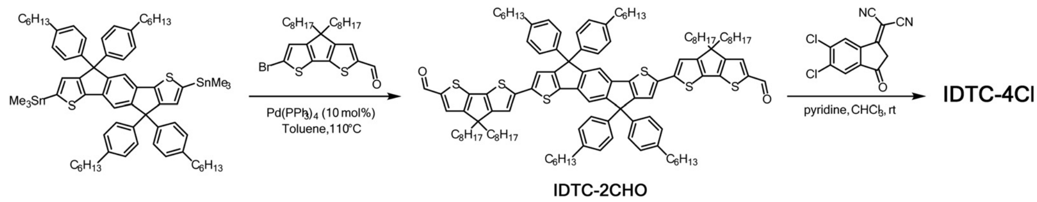

Fig. 2 The synthetic route to **IDTC-4Cl**.

The energy levels of **IDTC-4Cl** were determined by electrochemical cyclic voltammetry (CV) referenced to the energy level of Fc/Fc^+ (−4.8 eV below the vacuum level) in thin films (Fig. S3, ESI†). As is shown in Fig. 1c, the highest occupied molecular orbital (HOMO) level and lowest unoccupied molecular orbital (LUMO) level of **IDTC-4Cl** are −5.50 and −3.79 eV, respectively. The comparatively high HOMO level and low LUMO level are predominantly caused by the introduction of DTC as bridge units and IC-2Cl as ending groups, respectively. The absorption and CV investigations together prove it a promising strategy to decrease the E_g^{opt}. Besides, the energy levels of **PBDB-T**, **IDTC-4Cl** and $PC_{71}BM$ exhibit cascade alignments, which can facilitate charge transport from donors to acceptors efficiently.

Density functional theory (DFT) (B3LYP/6-31G*) calculations were employed to evaluate the optimal molecular geometry and the frontier molecular orbitals. The optimized geometric structures (top-view and side-view) and the electron-state-density distributions in the molecular orbitals (LUMO and HOMO) are shown in Fig. 3a and b, demonstrating an almost planar molecular backbone with a dihedral angle of 0.15° between the central IDT core and the DTC unit, which would facilitate efficient charge transfer. The calculated HOMO and LUMO energy levels of **IDTC-4Cl** are −5.16 and −3.37 eV, respectively.

Photovoltaic performance

To investigate the photovoltaic performance of **IDTC-4Cl**, solution-processed OSCs were fabricated with the conventional configuration of ITO/PEDOT:PSS/**PBDB-T**:acceptors/PDINO/Al, where PEDOT:PSS and PDINO represents poly(3,4-ethylenedioxythiopene):poly(styrenesulfonate) and perylene diimide functionalized with amino *N*-oxide, respectively. PDINO was selected as the cathode interlayer for effectively alleviating the interfacial energy barriers and electron extraction ability.[41] After systematic optimization of the OSC devices, by utilizing chlorobenezne as the processing solvent, the optimal donor/acceptor (D/A) weight ratio for all blends is 1 : 1, and a tiny amount of 1-chloronapthalene (CN, 0.5% volume) was selected as the solvent additive to ameliorate the morphology. The current density–voltage (J–V) curves of the optimal devices are shown in Fig. 4a, and their corresponding photovoltaic parameters are summarized in Table 1. Accordingly, the **PBDB-T:IDTC-4Cl** based device achieved a V_{oc} of 0.822 V and a J_{sc} of 19.14 mA cm^{-2}. The energy loss (E_{loss}), defined as $E_{loss} = E_g^{opt} - eV_{oc}$ (where E_g^{opt} refers to the optical band gap of **IDTC-4Cl**), is as low as 0.535 eV. Note that while the photovoltaic performance of a binary system exhibits an overall PCE of 9.51%, its performance is limited by a low FF of 60.2%. In order to purse a better morphology and maintain its V_{oc}/low E_{loss} and J_{sc}, we chose $PC_{71}BM$ as the third component for the **PBDB-T:IDTC-4Cl** system to construct ternary organic solar cells. By fixing the weight ratio of D : A as 1 : 1, we altered the $PC_{71}BM$ and **IDTC-4Cl** dosage (Table S1, ESI†). In comparison with the binary cells, the optimized $PC_{71}BM$: **PBDB-T** : **IDTC-4Cl** (1 : 0.8 : 0.2) ternary device delivered an elevated FF from 60.2% to 65.6% and resulted in an overall better PCE of 10.41%, ascribing from the cascade alignment of their energy levels for more efficient charge transport. Meanwhile, in the optimal

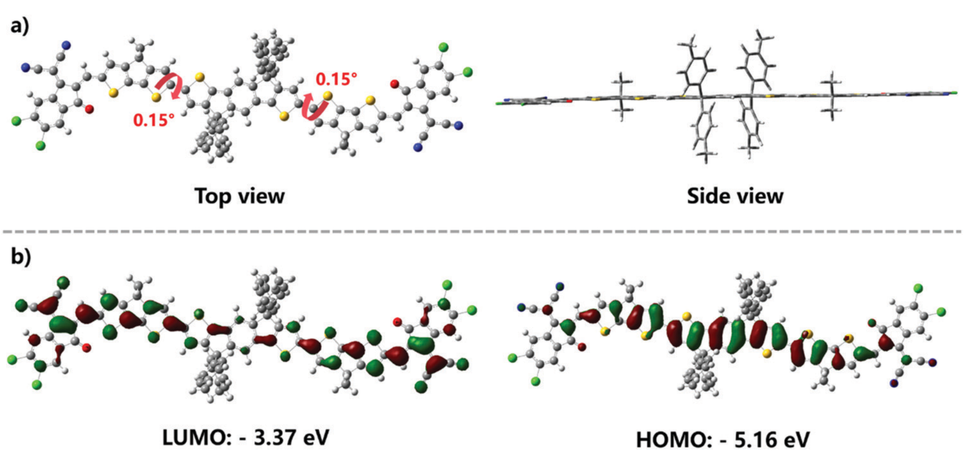

Fig. 3 (a) The optimized molecular geometry of BDTS-4Cl and BDTC-4Cl; (b) theoretical density distribution for the Frontier molecular orbitals *via* DFT-based theoretical calculations at the B3LYP/6-31G* level.

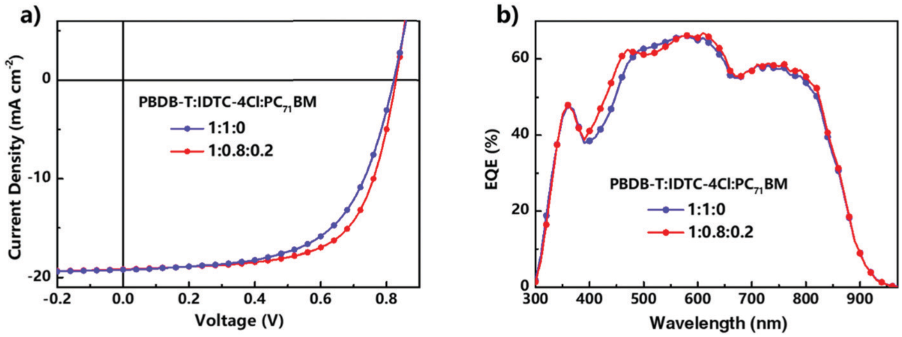

Fig. 4 (a) J–V and (b) EQE curves based on the binary and ternary devices.

Table 1 The optimal device parameters of the binary and ternary devices under the illumination of AM 1.5G (100 mW cm^{-2}) using the conventional device configuration

PBDB-T : IDTC-4Cl : $PC_{71}BM$	V_{oc} (eV)	J_{sc} (mA cm^{-2})	J_{cal} (mA cm^{-2})	FF (%)	PCE[a] (%)	E_{loss}[b] (eV)
1 : 1 : 0	0.822	19.19	18.07	60.2	9.50	0.535
1 : 0.8 : 0.2	0.829	19.14	18.40	65.6	10.41	0.527

[a] The average values with standard deviations obtained from 20 devices. [b] $E_{loss} = E_g^{opt} - eV_{oc}$.

ternary OSCs, the V_{oc} and J_{sc} remained almost unchanged, and the E_{loss} further decreased to 0.527 eV simultaneously.

From the external-quantum-efficiency (EQE) curves of the binary and ternary devices as shown in Fig. 4b, the **IDTC-4Cl** based binary and ternary OSCs both covered wide photo-current responses from 300 to 900 nm, mainly owing to the complementary absorption of a wide bandgap of **PBDB-T** in the visible region and the NBG acceptor in the NIR spectra. The integrated current densities for the **PBDB-T:IDTC-4Cl** and ternary devices are 18.07 and 18.40 mA cm^{-2}, respectively, both of which are closely to the J_{sc} values obtained from the J–V curves.

The charge transport properties were examined by the space-charge-limited current (SCLC) method using electron-only and hole-only devices, respectively. As shown in Fig. S2 (ESI†), the electron mobility of the neat **IDTC-4Cl** film was measured to be 2.84×10^{-4} cm^{-2} V^{-1} s^{-1}. The calculated electron and hole mobilities for the **PBDB-T:IDTC-4Cl** based device are 2.54×10^{-4} and 1.62×10^{-4} cm^{-2} V^{-1} s^{-1}, respectively. After adding $PC_{71}BM$, the ternary blend obtained higher electron (2.95×10^{-4} cm^{-2} V^{-1} s^{-1}) and hole (1.76×10^{-4} cm^{-2} V^{-1} s^{-1}) mobilities simultaneously, in support of its higher FF compared with that of the binary device. Using $PC_{71}BM$ as a combinatory acceptor, the enhanced electron and hole mobilities may be caused due to several factors: (1) the cascade level energy alignments for more efficient charge transfer (more charge transfer channels); (2) the more ameliorative morphology with suitable domain size (as shown in TEM images of Fig. 6c and d).

The plots of photocurrent (J_{ph}) *versus* effective applied voltage (V_{eff}) curves were measured to investigate the exciton dissociation and charge collection properties in the binary and ternary devices, respectively (Fig. 5a).[42,43] $J_{ph} = J_L - J_D$, where J_L is the current density under illumination and J_D is the current density in the darkness. $V_{eff} = V_o - V_a$, where V_a is the applied voltage and V_o is the voltage at which J_{ph} is zero. As depicted, when V_{eff} exceeds over 1.5 V, the J_{ph} values for the two devices reach saturation (J_{sat}), indicating a minimal charge recombination at a higher voltage. The exciton dissociation probability $P(E, T)$ in the working devices could be estimated by calculating the value of J_{ph}/J_{sat}, where E and T represent the field and temperature respectively. Under the condition of short-circuit current,

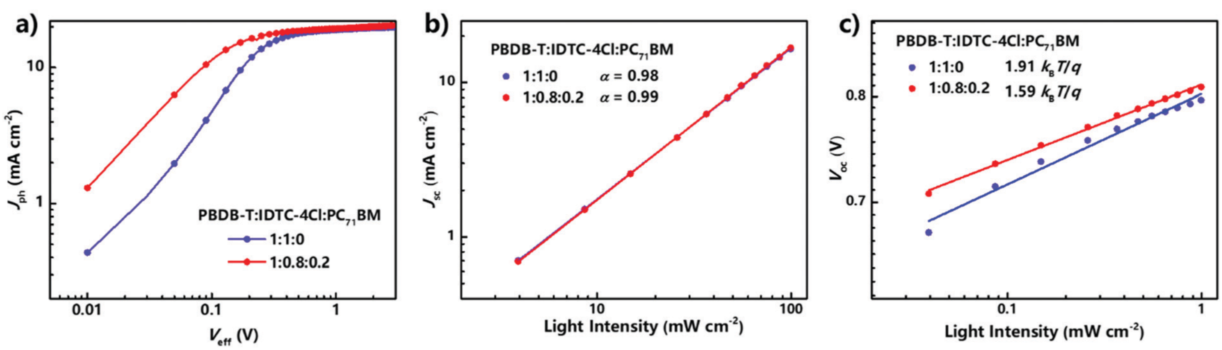

Fig. 5 (a) J_{ph} *versus* V_{eff}, (b and c) light-intensity dependence of J_{sc} and V_{oc} of their corresponding devices.

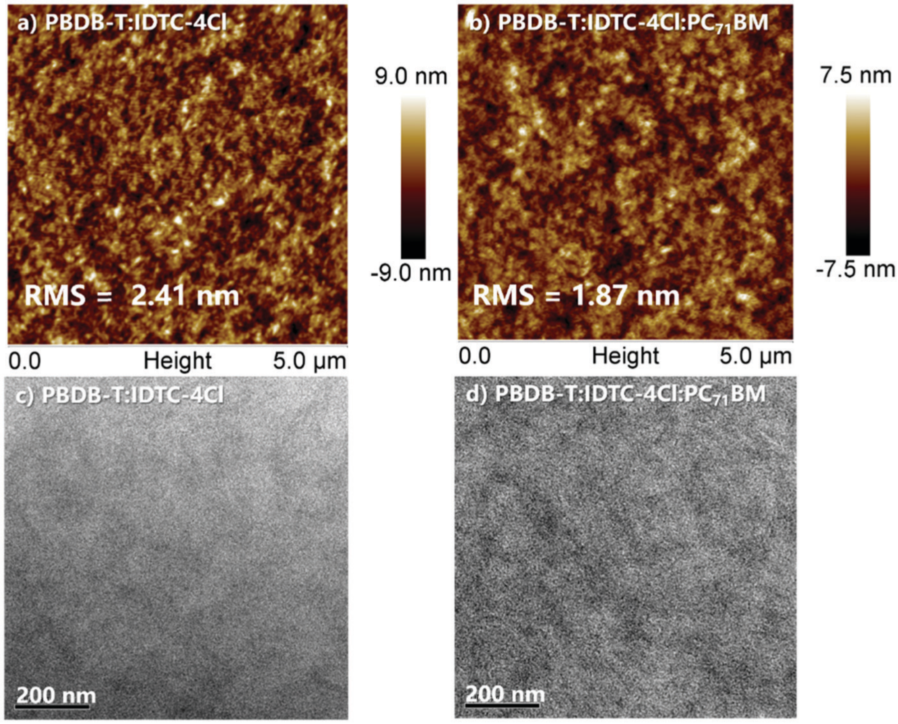

Fig. 6 (a and b) AFM height images and (c and d) TEM images of **IDTC-4Cl** based binary and ternary blends.

the $P(E, T)$ values are 95.1% and 94.2% for binary and ternary based devices, respectively, suggesting that the overall exciton dissociation and the charge collection processes are all quite efficient.

The light-intensity (P_{light}) dependence of J_{sc} was measured to further investigate the charge recombination properties in the devices (Fig. 5b). The power-law dependence between J_{sc} and P_{light} was described as $J_{sc}/P_{light}^{\alpha}$. The small deviation of the α value close to 1 indicates a weak bimolecular recombination. As seen, the α value for the binary and ternary devices are 0.98 and 0.99, respectively, indicating that the bimolecular recombination is efficiently suppressed in both the devices based on **IDTC-4Cl**.

In order to understand more about the recombination mechanism in the optimized devices, the dependence of V_{oc} on P_{light} was examined (Fig. 5c).[44,45] The slope of V_{oc} *versus* P_{light} helps to determine the degree of trap-assisted recombination in the working devices. A slope at k_BT/q implies that the bimolecular recombination mechanism is dominant, where k_B is Boltzmann's constant, T is the temperature and q is the elementary charge. As for trap-assisted or Shockley–Read–Hall (SRH) recombination, a stronger dependence of V_{oc} on light intensity with a slope of 2 k_BT/q is observed. As depicted, the slopes for the binary and ternary device based on **IDTC-4C**are at 1.91 and 1.59 k_BT/q, implying that the recombination at open circuit in these devices is a combination of monomolecular (SRH) and bimolecular processes.

Morphology characterization

To explore the morphological difference of a binary and ternary system, detailed investigations of the blend films were conducted by atomic force microscopy (AFM), and transmission electron microscopy (TEM) to evaluate the OPV peformance. As shown in Fig. 6a, the binary **PBDB-T:IDTC-4Cl** blend film exhibited good miscibility of the donor and acceptor components, with a root-mean-square surface roughness (R_q) of 2.41 nm. After adding the third component $PC_{71}BM$ (Fig. 6b), the ternary blend film showed a smoother surface with a R_q of 1.87 nm. The smoother and more uniform surface morphology of the ternary blend film, to certain extent, may favor for a modified contact between the electrode and the active layer. Compared with the **PBDB-T:IDTC-4Cl** blend film, the **PBDB-T:IDTC-4Cl**:$PC_{71}BM$ exhibited more defined fibrous and bi-continuous grain-like domains with appropriate size in the TEM images (Fig. 6c and d), benefitting charge carrier generation and transportation, which further accounts for the improved FF and thereby an enhanced performance of ternary OSCs.[46–48]

Conclusions

In summary, a cyclopentadithiophene-bridged A–D–A backboned SMA was designed and synthesized. Upon introduction of a DTC π-bridge along with a strong electron withdrawing end-group IC-2Cl, BDTC-4Cl exhibits a bandgap as low as 1.35 eV with near-infrared light absorption. In combination with **PBDB-T** as the polymer donor, the **IDTC-4Cl** based device gives a PCE of 9.51% with a V_{oc} of 0.822 V, FF of 60.2% and J_{sc} of 19.14 mA cm^{-2}. Upon introducing $PC_{71}BM$ as the third component, the ternary OSCs show an enhanced PCE of 10.41% with a much improved FF of 65.6% and slightly changed V_{oc} and J_{sc}. Considering the EQE response in a wide region of 300–900 nm, the introduction of a DTC unit in combination with the IC-2Cl terminal group, is a promising strategy to construct high performance SMAs with near-infrared light absorption.

Conflicts of interest

There are no conflicts to declare.

Acknowledgements

The authors gratefully acknowledge the financial support from National Natural Science Foundation of China (NSFC) (91633301, 51773095), the Ministry of Science and Technology of China (2016YFA0200200) and the Natural Science Foundation of Tianjin City (17JCJQJC44500, 17JCZDJC31100), 111 Project (B12015).

Notes and references

1 G. Yu, J. Gao, J. C. Hummelen, F. Wudl and A. J. Heeger, *Science*, 1995, **270**, 1789.
2 R. F. Service, *Science*, 2011, **332**, 293.
3 G. Li, R. Zhu and Y. Yang, *Nat. Photonics*, 2012, **6**, 153.
4 O. Ostroverkhova, *Chem. Rev.*, 2016, **116**, 13279.
5 Z. Xiao, X. Jia and L. Ding, *Sci. Bull.*, 2017, **62**, 1562.
6 B. Kan, H. Feng, H. Yao, M. Chang, X. Wan, C. Li, J. Hou and Y. Chen, *Sci. China: Chem.*, 2018, **61**, 1307.
7 L. Meng, Y. Zhang, X. Wan, C. Li, X. Zhang, Y. Wang, X. Ke, Z. Xiao, L. Ding, R. Xia, H. L. Yip, Y. Cao and Y. Chen, *Science*, 2018, **361**, 1094.
8 H. Zhang, H. Yao, J. Hou, J. Zhu, J. Zhang, W. Li, R. Yu, B. Gao, S. Zhang and J. Hou, *Adv. Mater.*, 2018, **30**, 1800613.
9 S. Zhang, Y. Qin, J. Zhu and J. Hou, *Adv. Mater.*, 2018, **30**, 1800868.
10 Y. Zhang, H. Yao, S. Zhang, Y. Qin, J. Zhang, L. Yang, W. Li, Z. Wei, F. Gao and J. Hou, *Sci. China: Chem.*, 2018, **61**, 1328.
11 A. Polman, M. Knight, E. C. Garnett, B. Ehrler and W. C. Sinke, *Science*, 2016, **352**, aad4424.
12 W. S. Yang, J. H. Noh, N. J. Jeon, Y. C. Kim, S. Ryu, J. Seo and S. I. Seok, *Science*, 2015, **348**, 1234.
13 Y. Chen, X. Wan and G. Long, *Acc. Chem. Res.*, 2013, **46**, 2645.
14 H. Feng, N. Qiu, X. Wang, Y. Wang, B. Kan, X. Wan, M. Zhang, A. Xia, C. Li, F. Liu, H. Zhang and Y. Chen, *Chem. Mater.*, 2017, **29**, 7908.
15 J. Hou, O. Inganas, R. H. Friend and F. Gao, *Nat. Mater.*, 2018, **17**, 119.
16 C. Yan, S. Barlow, Z. Wang, H. Yan, A. K. Y. Jen, S. R. Marder and X. Zhan, *Nat. Rev. Mater.*, 2018, **3**, 18003.
17 Y. Lin, J. Wang, Z. G. Zhang, H. Bai, Y. Li, D. Zhu and X. Zhan, *Adv. Mater.*, 2015, **27**, 1170.
18 H. Bin, Z. G. Zhang, L. Gao, S. Chen, L. Zhong, L. Xue, C. Yang and Y. Li, *J. Am. Chem. Soc.*, 2016, **138**, 4657.
19 S. Li, L. Ye, W. Zhao, S. Zhang, S. Mukherjee, H. Ade and J. Hou, *Adv. Mater.*, 2016, **28**, 9423.
20 Y. Lin, Q. He, F. Zhao, L. Huo, J. Mai, X. Lu, C. J. Su, T. Li, J. Wang, J. Zhu, Y. Sun, C. Wang and X. Zhan, *J. Am. Chem. Soc.*, 2016, **138**, 2973.
21 Y. Lin, F. Zhao, Q. He, L. Huo, Y. Wu, T. C. Parker, W. Ma, Y. Sun, C. Wang, D. Zhu, A. J. Heeger, S. R. Marder and X. Zhan, *J. Am. Chem. Soc.*, 2016, **138**, 4955.
22 Y. Yang, Z. G. Zhang, H. Bin, S. Chen, L. Gao, L. Xue, C. Yang and Y. Li, *J. Am. Chem. Soc.*, 2016, **138**, 15011.
23 S. Dai, F. Zhao, Q. Zhang, T. K. Lau, T. Li, K. Liu, Q. Ling, C. Wang, X. Lu, W. You and X. Zhan, *J. Am. Chem. Soc.*, 2017, **139**, 1336.
24 Z. Luo, H. Bin, T. Liu, Z. G. Zhang, Y. Yang, C. Zhong, B. Qiu, G. Li, W. Gao, D. Xie, K. Wu, Y. Sun, F. Liu, Y. Li and C. Yang, *Adv. Mater.*, 2018, **30**, 1706124.
25 Z. Luo, C. Sun, S. Chen, Z.-G. Zhang, K. Wu, B. Qiu, C. Yang, Y. Li and C. Yang, *Adv. Energy Mater.*, 2018, **8**, 1800856.
26 Z. Yao, X. Liao, K. Gao, F. Lin, X. Xu, X. Shi, L. Zuo, F. Liu, Y. Chen and A. K. Jen, *J. Am. Chem. Soc.*, 2018, **140**, 2054.
27 H. Yao, Y. Cui, R. Yu, B. Gao, H. Zhang and J. Hou, *Angew. Chem., Int. Ed.*, 2017, **56**, 3045.
28 Y. Cui, C. Yang, H. Yao, J. Zhu, Y. Wang, G. Jia, F. Gao and J. Hou, *Adv. Mater.*, 2017, **29**, 1703080.
29 H. Yao, Y. Chen, Y. Qin, R. Yu, Y. Cui, B. Yang, S. Li, K. Zhang and J. Hou, *Adv. Mater.*, 2016, **28**, 8283.
30 H. Bai, Y. Wu, Y. Wang, Y. Wu, R. Li, P. Cheng, M. Zhang, J. Wang, W. Ma and X. Zhan, *J. Mater. Chem. A*, 2015, **3**, 20758.
31 H. Lin, S. Chen, Z. Li, J. Y. Lai, G. Yang, T. McAfee, K. Jiang, Y. Li, Y. Liu, H. Hu, J. Zhao, W. Ma, H. Ade and H. Yan, *Adv. Mater.*, 2015, **27**, 7299.
32 S. Holliday, R. S. Ashraf, A. Wadsworth, D. Baran, S. A. Yousaf, C. B. Nielsen, C. H. Tan, S. D. Dimitrov, Z. Shang, N. Gasparini, M. Alamoudi, F. Laquai, C. J. Brabec, A. Salleo, J. R. Durrant and I. McCulloch, *Nat. Commun.*, 2016, **7**, 11585.
33 F. Liu, Z. Zhou, C. Zhang, T. Vergote, H. Fan, F. Liu and X. Zhu, *J. Am. Chem. Soc.*, 2016, **138**, 15523.
34 P. Cheng, M. Zhang, T. K. Lau, Y. Wu, B. Jia, J. Wang, C. Yan, M. Qin, X. Lu and X. Zhan, *Adv. Mater.*, 2017, **29**, 1605216.
35 W. Li, H. Yao, H. Zhang, S. Li and J. Hou, *Chem. – Asian J.*, 2017, **12**, 2160.
36 X. Li, T. Yan, H. Bin, G. Han, L. Xue, F. Liu, Y. Yi, Z.-G. Zhang, T. P. Russell and Y. Li, *J. Mater. Chem. A*, 2017, **5**, 22588.
37 F. Liu, Z. Zhou, C. Zhang, J. Zhang, Q. Hu, T. Vergote, F. Liu, T. P. Russell and X. Zhu, *Adv. Mater.*, 2017, **29**, 201606574.
38 Y. Z. Lin, Z. G. Zhang, H. T. Bai, J. Y. Wang, Y. H. Yao, Y. F. Li, D. B. Zhu and X. W. Zhan, *Energy Environ. Sci.*, 2015, **8**, 610.
39 S. Li, L. Zhan, F. Liu, J. Ren, M. Shi, C. Z. Li, T. P. Russell and H. Chen, *Adv. Mater.*, 2018, **30**, 1705208.
40 L. Zhan, S. Li, H. Zhang, F. Gao, T. K. Lau, X. Lu, D. Sun, P. Wang, M. Shi, C. Z. Li and H. Chen, *Adv. Sci.*, 2018, **5**, 1800755.
41 Z. G. Zhang, B. Y. Qi, Z. W. Jin, D. Chi, Z. Qi, Y. F. Li and J. Z. Wang, *Energy Environ. Sci.*, 2014, **7**, 1966.
42 P. W. M. Blom, V. D. Mihailetchi, L. J. A. Koster and D. E. Markov, *Adv. Mater.*, 2007, **19**, 1551.
43 C. M. Proctor, M. Kuik and T. Q. Nguyen, *Prog. Polym. Sci.*, 2013, **38**, 1941.

44 S. R. Cowan, A. Roy and A. J. Heeger, *Phys. Rev. B: Condens. Matter Mater. Phys.*, 2010, **82**, 245207.

45 L. J. A. Koster, V. D. Mihailetchi, R. Ramaker and P. W. M. Blom, *Appl. Phys. Lett.*, 2005, **86**, 123509.

46 H. Fu, Z. Wang and Y. Sun, *Angew. Chem., Int. Ed.*, 2018, **58**, 2.

47 L. Huo, T. Liu, X. Sun, Y. Cai, A. J. Heeger and Y. Sun, *Adv. Mater.*, 2015, **27**, 2938.

48 T. Liu, L. Huo, S. Chandrabose, K. Chen, G. Han, F. Qi, X. Meng, D. Xie, W. Ma, Y. Yi, J. M. Hodgkiss, F. Liu, J. Wang, C. Yang and Y. Sun, *Adv. Mater.*, 2018, **30**, 1707353.